Formation stability analysis of unmanned multi-vehicles under interconnection topologies

Yang, A., Naeem, W., & Fei, M. (2015). Formation stability analysis of unmanned multi-vehicles under interconnection topologies. International Journal of Control, 88(4), 754-767. DOI: 10.1080/00207179.2014.972465

Published in:
International Journal of Control

Document Version:
Peer reviewed version

International Journal of Control
Publication details, including instructions for authors and subscription information:
http://www.tandfonline.com/loi/tcon20

Formation stability analysis of unmanned multi-vehicles under interconnection topologies

Aolei Yang[a], Wasif Naeem[b] & Minrui Fei[a]

[a] Shanghai Key Laboratory of Power Station Automation Technology, School of Mechatronic Engineering and Automation, Shanghai University, 200072, Shanghai, P. R. China, +86 (0)21 56331634

[b] School of Electronics, Electrical Engineering and Computer Science, Queen's University Belfast, BT9 5AH, UK. +44 (0)28 90974066

Accepted author version posted online: 21 Oct 2014.

To cite this article: Aolei Yang, Wasif Naeem & Minrui Fei (2014): Formation stability analysis of unmanned multi-vehicles under interconnection topologies, International Journal of Control, DOI: 10.1080/00207179.2014.972465

To link to this article: http://dx.doi.org/10.1080/00207179.2014.972465

To appear in the *International Journal of Control*
Vol. 00, No. 00, Month 20XX, 1–21

Publisher: Taylor & Francis
Journal: *International Journal of Control*
DOI: http://dx.doi.org/10.1080/00207179.2014.972465

Formation stability analysis of unmanned multi-vehicles under interconnection topologies

Aolei Yang[a]*, Wasif Naeem[b] and Minrui Fei[a]

[a]Shanghai Key Laboratory of Power Station Automation Technology, School of Mechatronic Engineering and Automation, Shanghai University, 200072, Shanghai, P. R. China, +86 (0)21 56331634;
[b]School of Electronics, Electrical Engineering and Computer Science, Queen's University Belfast, BT9 5AH, UK. +44 (0)28 90974066
ayang02@qub.ac.uk; w.naeem@qub.ac.uk; mrfei@staff.shu.edu.cn

(*v4.0 released February 2014*)

Acknowledgement

This work was supported by the EPSRC under UK-China Science Bridge Grant (EP/G042594/1), Shanghai Municipal Commission of Economy and Informatization under Shanghai Industry-University-Research Collaboration Grant (CXY-2013-71), the Science and Technology Commission of Shanghai Municipality under "Yangfan Program" (14YF1408600), the National Natural Science Foundation of China (No. 61403244), and the Key Project of Science and Technology Commission of Shanghai Municipality under Grant (No. 14JC1402200).

*Corresponding author. Email: ayang02@qub.ac.uk

Abstract: In this paper, the overall formation stability of unmanned multi-vehicle is mathematically presented under interconnection topologies. A novel definition of formation error is first given and followed by the proposed formation stability hypothesis. Based on this hypothesis, a unique extension-decomposition-aggregation scheme is then employed to support the stability analysis for the overall multi-vehicle formation under a mesh topology. It is proved that the overall formation control system consisting of N number of nonlinear vehicles is not only asymptotically, but also exponentially stable in the sense of Lyapunov within a neighbourhood of the desired formation. This technique is shown to be applicable for a mesh topology but is equally applicable for other topologies. Simulation study of the formation manoeuvre of multiple Aerosonde UAVs, in 3D-space, is finally carried out verifying the achieved formation stability result.

Keywords: formation control; Lyapunov stability analysis; formation error; formation topology; formation stability hypothesis; unmanned aerial vehicle.

1. Introduction

The aim of multi-vehicle formation control problem is to control the displacement and/or attitude of each vehicle within some workspace to accomplish a common task. A group of vehicles can perform tasks faster and more efficiently compared to a single vehicle. For example, a multi-robot formation can be adopted to move a large object which may be impossible for a single robot; multiple unmanned aerial vehicles (UAVs) formation could achieve better area coverage for reconnaissance, thereby improving mission success. In recent years, research in formation flight control of multi-aircraft has attracted growing interest (Wu, Cao, Xing, Zheng, & Zhang, 2010). The implications of the formation flight are very significant, not just for fuel and energy saving but for future applications across civilian and military domains. For instance, formation flight can be used to handle the increase in air traffic around airports by means of civil aeroplane formation taking-off and landing to improve the efficiency of runway use (Murray, 2007).

A number of approaches have been proposed in the literature. The behaviour-based approach is decentralised and the control action of each element in the formation is a weighted average of the control for each behaviour (Balch & Arkin, 1998; Monteiro & Bicho, 2010). In the leader-following approach, the leader vehicle maintains a given trajectory while the followers track a fixed relative distance from the designated neighbouring vehicles (J. Wang & Wu, 2012; W. Wang & Slotine, 2006). The virtual structure approach is centralised and describes the whole formation as a single rigid body. Each vehicle has its own relative position in the body and tracks the desired trajectory which is translated from the desired motion of the rigid body (Askari, Mortazavi, & Talebi, 2013; Li & Liu, 2008). The standard artificial potential field (APF) approach is based on applying the negative gradient of an artificial potential function as control inputs to drive the overall formation to convergence (Do, 2007; Krick, Broucke, & Francis, 2009; Xue, Yao, Chen, & Yu, 2010). Further, a unified optimal control approach consisting of formation control, trajectory tracking, and obstacle avoidance was presented by J. Wang and Xin (2013) for multi-UAV coordination. Another novel formation control strategy: extension-decomposition-aggregation scheme was proposed by Yang, Naeem, Irwin, and Li (2014), and it is decentralised and the main idea is of translating the complex formation control problem into the stability problem of a group of individual augmented subsystems (IASs) which are simpler to be solved.

1.1 *Approaches to formation stability analysis*

Any closed-loop formation control methodology must naturally be guaranteed to be stable, especially where there is a potential of loss of human life and property. Most research papers in this area make use of either algebraic graph theory or Lyapunov stability theory.

The use of graph theory in the analysis of interconnected systems is not new (Corfmat & Morse, 1976), and the current interest is in applying graph-theoretic concepts to the multi-vehicle formation problem. An application of graph theory was discussed by Fax and Murray (2004), where a directed

graph was used to represent the communication network and to relate its topology with formation stability. Desai, Ostrowski, and Kumar (2001) presented a framework for describing the behaviours of robots in a formation, representing possible control graphs and the coordination of transitions with formation changes from one geometry to another. Additionally, in Mesbahi and Hadaegh (2000), elementary graph theory and linear matrix inequalities (LMI) are combined with logic-based switching to shed light on the various control strategies which are feasible in the leader-following framework for formation flying of multiple spacecraft. Furthermore, graphs have also been applied to describe the interconnection topology in a formation to reflect the control structure, information flow, and error propagation, i.e. Lin, Wang, Han, and Fu (2014) presented an approach based on complex Laplacian and provided an original analysis for the relationship between complex graph Laplacians and graphical interconnection.

Lyapunov stability theory is an alternative way to analyse the overall formation stability. In the paper (Ögren, Egerstedt, & Hu, 2002), a formation Lyapunov stability function was defined as a weighted sum of the control Lyapunov function for each vehicle to support the formation stability analysis. The idea of relative-position-based formation stability was proposed by Xue et al. (2010),and the Lyapunov method was also used to design the decentralised controllers, along with an extended LMI to analyse the conditions required for formation stability. Moreover, Hong, Gao, Cheng, and Hu (2007) proposed a Lyapunov-based approach to give a sufficient condition to make all the agents converge to a common value, and a common Lyapunov function was explicitly constructed in the case of switching jointly connected topologies. Dörfler and Francis (2010) analysed the asymptotic stability of minimally infinitesimally rigid formations using Lyapunov-based stability method, and also achieved the global asymptotic stability of triangular formations. In another paper (Feddema, Lewis, & Schoenwald, 2002), a combination of the above two strategies was employed, where a few concepts from graph theory were borrowed to evaluate the controllability and observability of the individual system and a vector Lyapunov method was then applied to prove the stability of the multi-vehicle formation.

1.2 *Contribution of this paper*

In this paper, a formation stability hypothesis and the relevant analysis procedure are presented in detail to provide a new approach for studying the formation stability. Based on this hypothesis, the extension-decomposition-aggregation (EDA) scheme (Yang et al., 2014) is employed to support the stability analysis of the overall multi-vehicle formation under an interconnection topology: mesh formation topology. The employed mesh topology is a robust formation topology, since it does not cause the entire formation to instability even if several links in the topology become unstable. In addition, if the formation is to be expanded, it can be done without causing formation disruption to the current multi-vehicle group.

For employing the EDA scheme, a coupled-multiple-pendulum system is designed to be a feasible candidate for the *virtual* additional system (VAS), and the formation stability analysis under a mesh formation topology is conveniently carried out by using Lyapunov stability theory. It is concluded that if all the designed individual augmented subsystems (IASs) can be stabilised, the overall formation system with a mesh topology is not only asymptotically, but also exponentially stable in the sense of Lyapunov within a neighbourhood of the desired formation.

In contrast to Yang et al. (2014), the stability analysis in this paper is based on the mesh interconnection topology, which is more complex than the chain topology (each vehicle has at most two neighbouring vehicles). Based on this complex interconnection topology, the relevant local and global formation errors (LFE and GFE) are defined. This is further supported by stability analysis and simulation experiments. In addition, the formation stability hypothesis is first presented in detail, and the EDA scheme proposed earlier is only considered as an implementation of stage one of this hypothesis. A nonlinear model is employed herein to verify the formation stability hypothesis and to carry out stability analysis. The complex nonlinear *Aerosonde* UAV model is subsequently adopted to support the multi-UAVs formation flight in simulations and to verify the

achieved formation stability result.

It is noted that interested readers are referred to Yang, Naeem, Irwin, and Li (2012b), Yang et al. (2014) and Yang, Naeem, Irwin, and Li (2012a) for a comprehensive treatment of some of the concepts used in this paper. However, some repetition in this paper is deemed necessary to fully understand the contribution of this work.

The remainder of the paper is organised as follows. Section 2 outlines the problem formulation. Section 3 presents the formation stability hypothesis and its specific EDA scheme, whilst Section 4 analyses the relevant stability of the overall formation system. Extensive simulation results are presented in Section 5 to illustrate the feasibility and verify the formation stability. The paper finally concludes with some discussion and suggestions for future work.

2. Problem formulation

As presented in Yang et al. (2014), a complete formation definition (**FD**) in Euclidean space should consist of the relative distances and the states of all the vehicles. Here, $\tilde{\mathbf{x}}_i$ denotes the state of the i^{th} vehicle, whilst the overall state of the formation system with N vehicles is defined as a vector $\tilde{\mathbf{x}} = [\tilde{\mathbf{x}}_1; \tilde{\mathbf{x}}_2; \cdots; \tilde{\mathbf{x}}_i; \cdots; \tilde{\mathbf{x}}_N]$ by combining the states of all the individual vehicles. Taking these into account, the **FD** is expressed as (1), in terms of the relative distances and states of individual vehicles.

$$\begin{aligned} \mathbf{FD}: \quad & F_{real} = \{\mathbf{r}_{ij} : i, j = 1, \cdots, N; i \neq j\} \\ & \tilde{\mathbf{x}} = [\tilde{\mathbf{x}}_1; \tilde{\mathbf{x}}_2; \cdots; \tilde{\mathbf{x}}_i; \cdots; \tilde{\mathbf{x}}_N] \end{aligned} \tag{1}$$

where the subscript "*real*" represents the real-time formation, and "$\mathbf{r}_{ij}$" means the relative distance between the i^{th} vehicle and the j^{th} vehicle.

Similar to the state definition $\tilde{\mathbf{x}}$, the input vector of the overall formation system is defined as $\tilde{\mathbf{u}} = [\tilde{\mathbf{u}}_1; \tilde{\mathbf{u}}_2; \cdots; \tilde{\mathbf{u}}_i; \cdots; \tilde{\mathbf{u}}_N]$ which consists of input vectors of all the individual vehicles.

2.1 *Definition of formation error under interconnection topologies*

There in general exist two kinds of formation errors in the literature. The one is local formation error (LFE) which is associated with each individual vehicle in a given formation geometry, and the other is called as global formation error (GFE) which is the summation of each vehicle's LFE. Here, the LFE is redefined based on the adopted interconnection formation topology, followed by the definition of the associated GFE.

An illustration of a mesh formation topology with both unidirectional and bidirectional reactions is shown in Fig. 1. Note that the word "reaction" is defined in this paper to demonstrate a response of an individual vehicle with respect to changes in the states of other vehicles. The direction of the reaction is identical to the direction of the corresponding communication topology.

By using denotation of digraph in graph theory, the formation status in Fig. 1 is mathematically expressed by $\mathbf{D} = (\mathbf{V}, \mathbf{E})$, where the position set $\mathbf{V}$ and the formation topology set $\mathbf{E}$ are given by (2),

$$\begin{aligned} \mathbf{V} &= \{\mathbf{p}_{L1}, \mathbf{p}_{L2}, \mathbf{p}_{L3}, \mathbf{p}_{L4}, \mathbf{p}_{L5}\}; \\ \mathbf{E} &= \{\mathrm{T}^{\mathrm{F}}_{1\leftrightarrow 2}, \mathrm{T}^{\mathrm{F}}_{1\leftrightarrow 3}, \mathrm{T}^{\mathrm{F}}_{2\leftrightarrow 3}, \mathrm{T}^{\mathrm{F}}_{2\leftrightarrow 4}, \mathrm{T}^{\mathrm{F}}_{4\to 3}, \mathrm{T}^{\mathrm{F}}_{4\leftrightarrow 5}, \mathrm{T}^{\mathrm{F}}_{5\to 3}\} \end{aligned} \tag{2}$$

where $\mathbf{p}_{Li} = (p_{Lix}, p_{Liy}, p_{Liz})$, $i = 1, 2, 3, 4, 5$, denotes the vehicle position in the local formation coordinate system (LFCS) which is defined in Yang et al. (2014), and $\mathrm{T}^{\mathrm{F}}_{i\leftrightarrow j}$ or $\mathrm{T}^{\mathrm{F}}_{i\to j}$ represents the corresponding reaction relationship. For vehicle 3, for instance, vehicles $1, 2, 4, 5$ are called as its **local reaction vehicles**(LRV), and the labels $\mathrm{w}_{1\to 3}$, $\mathrm{w}_{2\to 3}$, $\mathrm{w}_{4\to 3}$, $\mathrm{w}_{5\to 3}$ denote the **weighting**

values corresponding to the related vehicles. The LFE of the 3^{rd} vehicle, $e_{\mathrm{v}3}$ is then defined as (3),

$$\begin{aligned} e_{\mathrm{v}3}(\tilde{\mathbf{x}}_3) &= \frac{\sum_{j=1,j\neq 3}^{5} \mathrm{w}_{j\to 3}\left[(\mathbf{p}^r_{Lj}-\mathbf{p}^r_{L3})-(\mathbf{p}^d_{Lj}-\mathbf{p}^d_{L3})\right]}{\sum_{j=1,j\neq 3}^{5} \mathrm{w}_{j\to 3}} \\ &= \frac{\sum_{j=1,j\neq 3}^{5} \mathrm{w}_{j\to 3}(\mathbf{p}^r_{Lj}-\mathbf{p}^d_{Lj})}{\sum_{j=1,j\neq 3}^{5} \mathrm{w}_{j\to 3}} - (\mathbf{p}^r_{L3}-\mathbf{p}^d_{L3}) \end{aligned} \tag{3}$$

where $\mathbf{p}^r_{Lj}$ and $\mathbf{p}^d_{Lj}$ denote the real-time and desired positions of the j^{th} vehicles respectively, which are defined in the LFCS. The expression, $\mathbf{p}^r_{Li}-\mathbf{p}^d_{Li}$ is referred to as **isolated formation error** (IFE) for the i^{th} vehicle.

The relationship defined in (3) can be generalised to the i^{th} vehicle with M connected vehicles in a topology, and the general LFE for the i^{th} vehicle, $e_{\mathrm{v}i}$ is defined in (4),

$$e_{\mathrm{v}i}(\tilde{\mathbf{x}}_i) = \frac{\sum_{j} \mathrm{w}_{j\to i}(\mathbf{p}^r_{Lj}-\mathbf{p}^d_{Lj})}{\sum_{j} \mathrm{w}_{j\to i}} - (\mathbf{p}^r_{Li}-\mathbf{p}^d_{Li}) \tag{4}$$

where "j" is the index of the reaction vehicle relative to the current i^{th} vehicle, and $\mathrm{w}_{j\to i}$ denotes the relevant weighting value which is determined by the i^{th} vehicle according to the degree of the importance of the j^{th} vehicle. As given by (4), the proposed LFE for each vehicle in a topology can be alternatively described as: *the difference between the IFEs' weighted average of all the LRVs in the formation and the IFE of the current vehicle.*

Note that the weighting value of each vehicle can be assigned based on a rule. For instance, in order to support the obstacle avoidance, the rule can be described as: the closer the proximity between vehicles, the larger the weighting value. In this paper, all the weighting values are assumed to be equal to ***unity*** for simplicity.

The GFE, $\mathbf{e}_G$ with the formation topology is defined by (5),

$$\mathbf{e}_G(\tilde{\mathbf{x}},\tilde{\mathbf{u}}) = \sum_{i=1}^{N}(\|e_{\mathrm{v}i}(\tilde{\mathbf{x}}_i)\| + \|\tilde{\mathbf{u}}_i\|^2) \tag{5}$$

where $e_{\mathrm{v}i}(\tilde{\mathbf{x}}_i)$ is the IFE of the i^{th} vehicle and the term, $\|\tilde{\mathbf{u}}_i\|^2$ is a penalty on the inputs.

2.2 *Formation stability definition*

From the aforementioned definitions, a common and intuitive definition to formation stability is now presented below.

Formation stability definition 1: the formation with N vehicles is asymptotically stable in the sense of Lyapunov if (6) is satisfied (Murray, 2007),

$$\lim_{t\to+\infty} \|\mathbf{e}_G(\tilde{\mathbf{x}},\tilde{\mathbf{u}}) - \mathbf{e}_e\| = 0 \tag{6}$$

where t is the elapsed time, $\mathbf{e}_G(\tilde{\mathbf{x}},\tilde{\mathbf{u}})$ defined by (5) is also called as *cumulative formation error*,

and $\mathbf{e}_e$ represents the equilibrium value of $\mathbf{e}_G(\tilde{\mathbf{x}}, \tilde{\mathbf{u}})$. From the viewpoint of optimisation, $\mathbf{e}_e = min\{\mathbf{e}_G(\tilde{\mathbf{x}}, \tilde{\mathbf{u}})\}$.

Note that this definition only illustrates the formation stability in the global perspective, and it is in general inconvenient to carry out analysing the decentralised formation stability under the formation topology. Hence it is necessary to propose a further definition.

Formation stability definition 2: the formation with N vehicles is asymptotically stable in the sense of Lyapunov if both (7) and (8) are satisfied,

$$\lim_{t\to+\infty} \|F_{real} - F_e\| = 0 \tag{7}$$

$$\lim_{t\to+\infty} \|\tilde{\mathbf{x}} - \tilde{\mathbf{x}}_e\| = 0 \tag{8}$$

where t is the elapsed time, F_e indicates the equilibrium shape/geometry of the overall formation, and $\tilde{\mathbf{x}}_e = [\tilde{\mathbf{x}}_{e_1}; \tilde{\mathbf{x}}_{e_2}; \cdots; \tilde{\mathbf{x}}_{e_N}]$ consists of the equilibrium states of $\tilde{\mathbf{x}}_i, i = 1, 2, \cdots, N$. This formation stability definition means that the states of all the vehicles as well as the relative distances between them should converge to steady states.

It is obvious that F_{real} in (7) is a global representation of the overall formation. For an adopted decentralised control architecture, it is assumed that F_{real} can be decomposed into a set of local-formation representations, i.e.

$$F_{real} \triangleq \{F_{real_1}, F_{real_2}, \cdots, F_{real_i}, \cdots, F_{real_N}\} \tag{9}$$

where F_{real_i} corresponds to the local-formation representation of the i^{th} vehicle. Further, suppose that it can be expressed by a vector $\mathbf{x}_{F_{real_i}}$ to reflect the variations in the associated local-formation, the state vector $\tilde{\mathbf{x}}_i$ of the i^{th} vehicle can then be augmented as:

$$\mathbf{x}_i = [\tilde{\mathbf{x}}_i^T, \mathbf{x}_{F_{real_i}}^T]^T \tag{10}$$

where $\mathbf{x}_i$ is considered as the augmented state vector derived from the original one, $\tilde{\mathbf{x}}_i$ of the i^{th} vehicle. Based on this, ***Formation stability definition 2*** is then redefined as follows.

Formation stability definition 3: the formation with N vehicles is asymptotically stable in the sense of Lyapunov if (11) is satisfied,

$$\lim_{t\to+\infty} \|\mathbf{X} - \mathbf{X}_e\| = 0 \tag{11}$$

where $\mathbf{X} = [\mathbf{x}_1; \mathbf{x}_2; \cdots; \mathbf{x}_i; \cdots; \mathbf{x}_N]$ consists of all the state vectors of the **augmented systems** derived from the original vehicle systems, and $\mathbf{X}_e = [\mathbf{x}_{e_1}; \mathbf{x}_{e_2}; \cdots; \mathbf{x}_{e_i}; \cdots; \mathbf{x}_{e_N}]$ denotes the equilibrium states including all the individual equilibrium states of the augmented systems. It is noted that although the above three definitions show different forms, in essence, they are equivalent each other.

3. Formation stability hypothesis and EDA strategy

Formation stability hypothesis*: the overall formation system is guaranteed to be stable if the following three requirements are satisfied.*

(1) There exists a group of dynamic systems (DSs) *which are augmented versions of corresponding original vehicles.*

(2) All the DSs *interacting with each other completely constitute the overall formation control system.*

(3) Each individual DS *can be stabilised by the respective decentralised controller.*

The relationship between the hypothesis and the analysis of the formation stability is intuitively shown in Fig. 2, where Stage 2 is supported by the formation stability definition 3, and Stage 1 will be specified and implemented in this section. It is noted that the DS represents a system which is needed to be determined or designed. Recalling the definition of the augmented states in (11), a DS can be considered as the augmented system of each original vehicle, and the combination of states of all the DSs can also be denoted by $\mathbf{X} = [\mathbf{x}_1; \mathbf{x}_2; \cdots; \mathbf{x}_i; \cdots; \mathbf{x}_N]$, where $\mathbf{x}_i$ means the augmented state vector of the i^{th} DS. If all the DSs can be stabilised by their decentralised controllers, it means that the stability requirement in (11) is guaranteed, and consequently the whole formation system is stable.

If this hypothesis is assumed to be correct, the process of the overall formation stability analysis can be carried out as follows:

(1) Attempt to seek or determine feasible DSs according to a desired specification.
(2) Design individual controllers to stabilise all the achieved DSs.
(3) Carry out simulation analysis to verify the performance of the overall formation system. If the achieved performance does not meet with the desired target, return to Step 1.
(4) If the performance in Step 3 is satisfactory, analyse the stability of the whole formation mathematically.

Note that since different DSs will present different characteristics of the overall formation system, the aim of the first three steps is to *seek or construct* plausibly feasible DSs. Only achieving these DSs can the overall formation stability be mathematically analysed in Step 4.

Based on the above hypothesis and the subsequent procedure, the extension-decomposition-aggregation (EDA) scheme proposed in Yang et al. (2012b) is employed to implement the Stage 1 of the hypothesis. The framework of the EDA scheme is illustrated in Fig. 3.

In the **extension** process, a *virtual* additional system (VAS) is employed to build the relationship between isolated vehicles and to produce an overall formation system involving formation information. **Decomposition** to the overall formation system is then carried out to translate the complex formation system into a group of feasible subsystems interacting via boundary conditions. Here, such decomposed subsystems are referred to as individual augmented subsystem (IASs) which is the implementation of the DSs. A scalar Lyapunov function is next selected as an index for representing the stability of each IAS. These indices are finally **aggregated** to mathematically analyse the subsystem interactions and the stability of the overall formation using Lyapunov stability theory.

Broadly speaking, the N IASs are associated with the N scalar Lyapunov functions $(V_i, i = 1, 2, \cdots, N)$, where each determines the stability property of an individual IAS. These scalar functions are considered as the components of the overall Lyapunov function $\mathbf{V}$. A differential inequality is formed in terms of this function, using the original inequalities of the decomposed IASs. The stability of the overall formation control system can then be determined by considering only the differential inequalities involving the N Lyapunov functions.

For the typical formation control approaches, i.e. behaviour-based, virtual structure, leader-following and artificial potential approaches, the stability analysis is generally derived by carrying out some or all of the following steps in this order: (1) propose a formation control problem, (2) explore a strategy to solve it, (3) analyse formation stability based on the proposed strategy, and (4) design formation controllers to meet the desired requirement or specification. However, in this paper, the formation stability hypothesis is first proposed based on the decentralized formation control framework, and the following work is to verify the hypothesis. Based on the hypothesis and its corresponding necessary assumptions presented above, the EDA scheme is employed to implement Stage 1 of the hypothesis. This EDA scheme is a novel approach to analyse the stability of complex networked systems which is originally proposed by augmenting the well-known "decomposition-aggregation" (DA) approach usually employed to analyse the stability of high-dimensional complex systems. In other words, the DA approach was extended and a relationship

was constructed between the EDA scheme and the formation stability hypothesis.

4. Formation stability analysis

In order to construct a group of feasible DSs or IASs, a VAS is designed before carrying out the formation stability analysis. Here, a coupled-multiple-pendulum (CMP) is adopted as the VAS as opposed to a coupled-multiple-inverted-pendulum (CMIP) system used in Yang et al. (2014). Although these two models are very similar in concept, they have different dynamic and stability characteristics. For instance the CMIP is intrinsically an unstable system with faster dynamic response, whereas the CMP is inherently a stable system with relatively slower dynamics. Additionally, this demonstrates the use of other systems as the VAS in this context.

Taking into account a full-mesh topology, a CMP system consists of N cart-mounted hanging pendulums coupled by $N(N-1)/2$ interactions. Fig. 4 shows interconnections between the i^{th} pendulum and others using the mesh topology.

The relationship between the above CMP and a multi-vehicle formation system can be intuitively explained by analogy with the motion of each cart of the CMP system. One approach of constructing the relationship is to consider an interaction exerted by a "virtual spring" between two pendulums as the communication channel between two vehicles. The natural lengths of springs are then considered as the desired formation parameters or variables (Yang et al., 2014). If a formation is not stable, the force or torque exerted by the springs must then impact the pendulums and result in a change in their deflection angles ε_i. This implies that the variation of ε_i is a reflection or indication of the formation error and it is referred to as a **local-formation variable**. Thus, the main aim of the decentralised formation controller design can be translated into the regulation problem of the local-formation variable by manoeuvring the formation vehicles. These will automatically cause the virtual springs to return to their balanced states, i.e. the overall formation becomes stable.

The mathematical modeling and properties of the CMP system with a mesh topology will be detailed first to support the following formation stability analysis.

4.1 *Modelling and properties of CMP system*

In Fig. 4, the points p_{i-1}, p_i, p_{i+1}, p_{i+2} are the positions of the $(i-1)^{th}$, i^{th}, $(i+1)^{th}$, $(i+2)^{th}$ carts respectively, and the points s_{i-1}, s_i, s_{i+1}, s_{i+2} denote the corresponding force points where the interactions exist. Note that $F_{i(i-1)}$, $F_{i(i+1)}$, $F_{i(i+2)}$ denote the forces on the i^{th} pendulum exerted by the interacting $(i-1)^{th}$, $(i+1)^{th}$, $(i+2)^{th}$ pendulums respectively.

The model of the i^{th} pendulum can be mathematically expressed by (12),

$$(I+ml^2)\ddot{\varepsilon}_i + B_c\dot{\varepsilon}_i = -ml\ddot{p}_i\cos\varepsilon_i - mgl\sin\varepsilon_i + \sum_{j=1,j\neq i}^{N} T_{ij} \tag{12}$$

where $I = ml^2/3$ is the moment of inertia for the pendulum, B_c is the viscous damping constant at the pivot point, ε_i stands for the deflection angle of the i^{th} pendulum from its vertical position (anti-clockwise rotation is positive), l and h are the lengths from the pivot to the centre of gravity of the pendulum and to the point where the interaction exist, m and g represent the mass and the gravitational constants respectively, and T_{ij} is the torque on the i^{th} pendulum exerted by the interacted j^{th} pendulum. The complete model of the CMP with the mesh topology is then given

by (13).

$$\begin{cases} (I+ml^2)\ddot{\varepsilon}_1 + B_c\dot{\varepsilon}_1 = -ml\ddot{p}_1\cos\varepsilon_1 - mgl\sin\varepsilon_1 + \sum\limits_{j=1,j\neq 1}^{N} T_{1j} \\ (I+ml^2)\ddot{\varepsilon}_2 + B_c\dot{\varepsilon}_2 = -ml\ddot{p}_2\cos\varepsilon_2 - mgl\sin\varepsilon_2 + \sum\limits_{j=1,j\neq 2}^{N} T_{2j} \\ \quad\vdots \\ (I+ml^2)\ddot{\varepsilon}_i + B_c\dot{\varepsilon}_i = -ml\ddot{p}_i\cos\varepsilon_i - mgl\sin\varepsilon_i + \sum\limits_{j=1,j\neq i}^{N} T_{ij} \\ \quad\vdots \\ (I+ml^2)\ddot{\varepsilon}_N + B_c\dot{\varepsilon}_N = -ml\ddot{p}_N\cos\varepsilon_N - mgl\sin\varepsilon_N + \sum\limits_{j=1,j\neq N}^{N} T_{Nj} \end{cases} \tag{13}$$

If all the individual pendulum systems are stable and operating around the nominal conditions, then $\ddot{\varepsilon}_i = 0$, $\dot{\varepsilon}_i = 0$ and $\ddot{p}_i = 0$, $(i = 1, 2, \cdots, N)$. The following result is then obtained by adding the two sides of equation (13).

$$\sum_{j=1,j\neq 1}^{N} T_{1j} + \sum_{j=1,j\neq 2}^{N} T_{2j} + \cdots + \sum_{j=1,j\neq N}^{N} T_{Nj} - mgl(\sin\varepsilon_1 + \sin\varepsilon_2 + \cdots \sin\varepsilon_N) = 0 \tag{14}$$

In order to simplify the mathematical description, Fig. 5(A) demonstrates a case with 4 pendulums, and the 2^{nd} pendulum is chosen as the object of study. Provided that all the individual pendulum systems are stable, i.e. the relevant pendulums maintain their torque balanced conditions, there exist the following equations given by (15).

$$\begin{aligned} T_{12} + T_{13} + T_{14} &= mgl\sin\varepsilon_1 \\ T_{21} + T_{23} + T_{24} &= mgl\sin\varepsilon_2 \\ T_{31} + T_{32} + T_{34} &= mgl\sin\varepsilon_3 \end{aligned} \tag{15}$$

Fig. 5(B) shows another equivalent structure of Fig. 5(A) with the 2^{nd} pendulum decomposed into three equivalent pendulums A, B and C. Each one is then used to equivalently balance the corresponding pendulum. In order to maintain the torque balance of the 2^{nd} pendulum in Fig. 5(B), its resultant torque should satisfy equation (16).

$$\begin{aligned} &-(-\hat{F}_{12})h\cos(-\varepsilon_1) - (-\hat{F}_{32})h\cos(-\varepsilon_3) - (-\hat{F}_{42})h\cos(-\varepsilon_4) \\ &+ mgl\sin(-\varepsilon_1) + mgl\sin(-\varepsilon_3) + mgl\sin(-\varepsilon_4) = 0 \end{aligned} \tag{16}$$

The sum of the first three terms on the left of (16) is the resultant torque exerted by all the interactions. Recalling the second equation in (15), the following equation shown in (17) holds.

$$\begin{aligned} &-(-\hat{F}_{12})h\cos(-\varepsilon_1) - (-\hat{F}_{32})h\cos(-\varepsilon_3) - (-\hat{F}_{42})h\cos(-\varepsilon_4) \\ &= -(T_{21} + T_{23} + T_{24}) \\ &= -mgl\sin\varepsilon_2 \end{aligned} \tag{17}$$

Combining (16) and (17) generates the equation:

$$\sin\varepsilon_1 + \sin\varepsilon_2 + \sin\varepsilon_3 + \sin\varepsilon_4 = 0 \tag{18}$$

Using the above method, a similar result can be obtained for N pendulums as given by (19).

$$\sin\varepsilon_1 + \sin\varepsilon_2 + \sin\varepsilon_3 + \cdots + \sin\varepsilon_N = 0 \tag{19}$$

Combining (14) and (19) yields (20),

$$\sum_{j=1,j\neq 1}^{N} T_{1j} + \sum_{j=1,j\neq 2}^{N} T_{2j} + \cdots + \sum_{j=1,j\neq N}^{N} T_{Nj} = 0 \tag{20}$$

which shows crucially that if all the individual pendulums are stable, the resultant torque of the whole CMP is zero whatever the interconnection topology is. This useful result will be used to support the stability analysis of the multi-vehicle formation.

4.2 *Formation stability analysis under mesh topology*

It is assumed that the overall formation system, $\mathbf{S}$ consisting of the CMP system can be decomposed into N coupled nonlinear subsystems or IASs, $\mathbf{S}_i, (i = 1, 2, \cdots, N)$, as shown in (21),

$$\mathbf{S}: \begin{cases} \mathbf{S}_1 : \dot{\mathbf{x}}_1 = f(t, \mathbf{x}_1) + \sum\limits_{j=1,j\neq 1}^{N} h_{1j} \\ \mathbf{S}_2 : \dot{\mathbf{x}}_2 = f(t, \mathbf{x}_2) + \sum\limits_{j=1,j\neq 2}^{N} h_{2j} \\ \vdots \\ \mathbf{S}_i : \dot{\mathbf{x}}_i = f(t, \mathbf{x}_i) + \sum\limits_{j=1,j\neq i}^{N} h_{ij} \\ \vdots \\ \mathbf{S}_N : \dot{\mathbf{x}}_N = f(t, \mathbf{x}_N) + \sum\limits_{j=1,j\neq N}^{N} h_{Nj} \end{cases} \tag{21}$$

where $f(t, \mathbf{x}_i)$ is an analytic function modelling the nonlinear dynamics of the i^{th} vehicle, $\sum\limits_{j=1,j\neq i}^{N} h_{ij}$ describes the resultant interactions of the i^{th} IAS with all the other IASs which are dependent on the topology, i.e. mesh in this case. Now consider the stability of the corresponding decoupled IASs $\tilde{\mathbf{S}}_1, \tilde{\mathbf{S}}_2, \cdots, \tilde{\mathbf{S}}_N$ by ignoring the above interactions.

$$\begin{aligned} &\tilde{\mathbf{S}}_1 : \dot{\mathbf{x}}_1 = f(t, \mathbf{x}_1); \\ &\tilde{\mathbf{S}}_2 : \dot{\mathbf{x}}_2 = f(t, \mathbf{x}_2); \\ &\vdots \\ &\tilde{\mathbf{S}}_N : \dot{\mathbf{x}}_N = f(t, \mathbf{x}_N); \end{aligned} \tag{22}$$

Suppose that there exists a function $V_i(t, \mathbf{x})$ for the i^{th} IAS, such that $V_i(t, \mathbf{0}) \equiv 0$ and

$$\begin{cases} c_{i1} \|\mathbf{x}_i\| \leq V_i(t, \mathbf{x}_i) \leq c_{i2} \|\mathbf{x}_i\| \\ \dot{V}_i(t, \mathbf{x}_i) \leq -c_{i3} \|\mathbf{x}_i\| \\ \|grad\ \ V_i(t, \mathbf{x}_i)\| \leq c_{i4} \end{cases} \tag{23}$$

where c_{i1}, c_{i2}, c_{i3} and c_{i4} are positive scalars depending on physical systems. The equilibrium states $\mathbf{x}_i^* = \mathbf{0}$ of $\tilde{\mathbf{S}}_i$ are then said to be exponentially stable globally (Khalil, 2001). Here, the chosen function $V_i(t, \mathbf{x})$ is referred to as a candidate Lyapunov function, and it is used as the stability index for each nonlinear subsystem $\tilde{\mathbf{S}}_i$. Furthermore, the derivative $\dot{V}_i$ along the solution of the i^{th} interacting IAS, $\mathbf{S}_i$ in (21) is given by (24).

$$\dot{V}_i = (grad\ V_i)^T \dot{\mathbf{x}}_i = (grad\ V_i)^T [f(t, \mathbf{x}_i) + \sum_{j=1, j\neq i}^{N} h_{ij}] \tag{24}$$

Note that the term, $(grad\ V_i)^T \cdot f(t, \mathbf{x}_i)$, is associated with the decoupled system (22), and the expression, $\|\mathbf{x}_i\| \geq c_{i2}^{-1} V_i(t, \mathbf{x}_i)$, follows from the first inequality in (23). So, there exists an inequality given by (25).

$$(grad\ V_i)^T \cdot f(t, \mathbf{x}_i) \leq -c_{i3} \|\mathbf{x}_i\| \leq -c_{i3} c_{i2}^{-1} V_i \tag{25}$$

The stability of the overall formation system, $\mathbf{S}$, is expressed by considering the interactions between these $V_i(t, \mathbf{x}_i), (i = 1, 2, \cdots, N)$. The function given in (26) defines a candidate Lyapunov function $\mathbf{V}(t, \mathbf{X})$ for $\mathbf{S}$, which is the weighted sum of all the individual Lyapunov functions,

$$\mathbf{V}(t, \mathbf{X}) = \sum_{i=1}^{N} k_i V_i(t, \mathbf{x}_i) = k_1 V_1(t, \mathbf{x}_1) + k_2 V_2(t, \mathbf{x}_2) + \cdots + k_N V_N(t, \mathbf{x}_N) \tag{26}$$

where $\mathbf{X} = [\mathbf{x}_1^T, \mathbf{x}_2^T, \cdots, \mathbf{x}_N^T]^T$ is defined by combining with the solutions of $\mathbf{S}_i, i = 1, 2, \cdots, N$, to represent a solution of the overall formation control system $\mathbf{S}$ in (21). In addition, the choice of coefficients $k_i, (i = 1, 2, \cdots, N)$ reflects differences in vehicle dynamics. Its time derivative $\dot{\mathbf{V}}(t, \mathbf{X})$ is now given in (27).

$$\begin{aligned} \dot{\mathbf{V}}(t, \mathbf{X}) &= k_1 \dot{V}_1(t, \mathbf{x}_1) + k_2 \dot{V}_2(t, \mathbf{x}_2) + \cdots + k_N \dot{V}_N(t, \mathbf{x}_N) \\ &= \sum_{i=1}^{N} k_i (grad\ V_i)^T f(t, \mathbf{x}_i) + \sum_{j=1, j\neq 1}^{N} k_1 (grad\ V_1)^T \cdot h_{1j} \\ &\quad + \sum_{j=1, j\neq 2}^{N} k_2 (grad\ V_2)^T \cdot h_{2j} + \cdots + \sum_{j=1, j\neq N}^{N} k_N (grad\ V_N)^T \cdot h_{Nj} \end{aligned} \tag{27}$$

By taking the norm on the right-hand side of (27) and using the estimates in (23) and (25), $\dot{\mathbf{V}}$ is then given by (28),

$$\begin{aligned} \dot{\mathbf{V}} &\leq \sum_{i=1}^{N} (-c_{i3} c_{i2}^{-1} k_i V_i) + \nabla_{max} k_{max} [\sum_{j=1, j\neq 1}^{N} h_{1j} + \sum_{j=1, j\neq 2}^{N} h_{2j} + \cdots + \sum_{j=1, j\neq N}^{N} h_{Nj}] \\ &\leq -c_{min} (k_1 V_1 + k_2 V_2 + k_3 V_3 + \cdots + k_N V_N) \\ &\quad + \nabla_{max} k_{max} [\sum_{j=1, j\neq 1}^{N} h_{1j} + \sum_{j=1, j\neq 2}^{N} h_{2j} + \cdots + \sum_{j=1, j\neq N}^{N} h_{Nj}] \end{aligned} \tag{28}$$

where $k_{max} = max\{k_1, k_2, \cdots, k_N\}$, $\nabla_{max} = max\{\|(grad\ V_1)^T\|, \|(grad\ V_2)^T\|, \cdots, \|(grad\ V_N)^T\|\}$ and $c_{min} = min\{c_{13} c_{12}^{-1}, c_{23} c_{22}^{-1}, \cdots, c_{N3} c_{N2}^{-1}\} > 0$.

Moreover, depending on the characteristics of the VAS, which is the multiple pendulum system in this case, the result achieved in (20) can be used to generate the equation given in (29) if all the decomposed IASs are stable. This is because the interactions $\sum_{j=1,j\neq i}^{N} h_{ij}$, $(i,j=1,2,\cdots,N)$ in (21) are the reflections of the reactions in the CMP system.

$$\sum_{j=1,j\neq 1}^{N} h_{1j} + \sum_{j=1,j\neq 2}^{N} h_{2j} + \cdots + \sum_{j=1,j\neq N}^{N} h_{Nj} = 0 \tag{29}$$

Incorporating (29) in (28), the following differential inequality is obtained.

$$\begin{aligned} \dot{\mathbf{V}} &\leq -c_{min}[k_1 V_1(t,\mathbf{x}_1) + k_2 V_2(t,\mathbf{x}_2) + \cdots + k_N V_N(t,\mathbf{x}_N)] \\ &= -c_{min}\mathbf{V} \end{aligned} \tag{30}$$

The above inequality is valid for all $t \geq t_0$, and its solution is given by (31),

$$\mathbf{V} \leq \mathbf{V}_0 \exp[-c_{min}(t-t_0)], \quad t \geq t_0 \tag{31}$$

where $\mathbf{V}_0 = \mathbf{V}(t_0,\mathbf{X}) = k_1 V_1(t_0,\mathbf{x}_1) + k_2 V_2(t_0,\mathbf{x}_2) + \cdots + k_N V_N(t_0,\mathbf{x}_N)$ is the initial value of $\mathbf{V}(t,\mathbf{X})$ for the overall formation system, and $V_i(t_0,\mathbf{x}_i)$ denotes the initial values corresponding to the i^{th} IAS $\mathbf{S}_i$. Then, using the first inequality in (23) for the functions $V_1(\mathbf{x}_1), V_2(\mathbf{x}_2), \cdots, V_N(\mathbf{x}_N)$, as well as the definition (26), the following inequalities hold,

$$\begin{aligned} \mathbf{V} &\geq k_1 c_{11} \|\mathbf{x}_1\| + k_2 c_{21} \|\mathbf{x}_2\| + \cdots + k_N c_{N1} \|\mathbf{x}_N\| \geq c_m (\|\mathbf{x}_1\| + \|\mathbf{x}_2\| + \cdots + \|\mathbf{x}_N\|) \\ \mathbf{V}_0 &\leq k_1 c_{12} \|\mathbf{x}_{10}\| + k_2 c_{22} \|\mathbf{x}_{20}\| + \cdots + k_N c_{N2} \|\mathbf{x}_{N0}\| \leq c_M (\|\mathbf{x}_{10}\| + \|\mathbf{x}_{20}\| + \cdots + \|\mathbf{x}_{N0}\|) \end{aligned} \tag{32}$$

where $c_m = min\{k_1 c_{11}, k_2 c_{21}, \cdots, k_N c_{N1}\} > 0$, $c_M = max\{k_1 c_{12}, k_2 c_{22}, \cdots, k_N c_{N2}\} > 0$, and $\mathbf{x}_{i0} = \mathbf{x}_i(t_0), i = 1,2,\cdots,N$, denote the initial states of all the IASs. As for the previously defined solution $\mathbf{X} = [\mathbf{x}_1^T, \mathbf{x}_2^T, \cdots, \mathbf{x}_N^T]^T$ of the whole formation system, the relationship between their norms is given by (33).

$$\|\mathbf{X}\| \leq \|\mathbf{x}_1\| + \|\mathbf{x}_2\| + \cdots + \|\mathbf{x}_N\| \leq \sqrt{2}\,\|\mathbf{X}\| \tag{33}$$

Combining (32) and (33) generates two inequalities,

$$\mathbf{V} \geq c_m \|\mathbf{X}\|, \quad \mathbf{V}_0 \leq \sqrt{2} c_M \|\mathbf{X_0}\| \tag{34}$$

and applying the above inequality to (31), produces the final result for showing the stability of the overall formation. Thus,

$$\begin{aligned} & c_m \|\mathbf{X}\| \leq \mathbf{V} \leq \sqrt{2} c_M \|\mathbf{X}_0\| \exp[-c_{min}(t-t_0)] \\ & \Rightarrow \|\mathbf{X}\| \leq \tfrac{\sqrt{2}c_M}{c_m} \|\mathbf{X}_0\| \exp[-c_{min}(t-t_0)] \\ & \Rightarrow \|\mathbf{X}\| \leq C \|\mathbf{X}_0\| \exp[-c_{min}(t-t_0)] \end{aligned} \tag{35}$$

where $t \geq t_0$, $C = \frac{\sqrt{2}c_M}{c_m} > 0$, and $\mathbf{X}$ is the solution of the whole system for the initial conditions $(t_0, \mathbf{X_0})$. Recalling the ***formation stability definition 3***, the inequality in (35) indicates that the solution of the overall formation system exponentially converges to the equilibrium point $\mathbf{X}_e = C\|\mathbf{X}_0\|$, which is in the neighbourhood of the desired formation.

In a word, the overall formation system with a mesh topology is not only asymptotically, but also exponentially stable in the sense of Lyapunov within a neighbourhood of the desired formation, if all the designed IASs are stable or can be stabilised.

5. Simulation Study

A nonlinear Simulink model (Baldonado, Chang, Gravano, & Paepcke, 2003) of the 6-DOF autonomous *Aerosonde* UAV is employed to support the multi-UAVs formation flight and to verify the achieved formation stability result. The *Aerosonde* UAV has a length of $1.74\,m$, a wingspan of $2.87\,m$, and maximum payload capacity of $5\,kg$. It was designed for applications including long-range weather data acquisition and reconnaissance over oceanic and remote areas.

The designed formation flight scenario is given as: all the UAVs were initially flying with the desired formation geometry in the mesh topology as shown in Fig. 6; the group of UAVs is tasked to navigate the 3-D waypoints provided in Table 1, whilst maintaining the formation topology and the reference 3-D formation geometry; the reference airspeed is $26\,m/s$, whereas the speed constraints are $15 \sim 50\,m/s$.

In Fig. 6, the labelled diamond symbol indicates the corresponding UAV, whereas UAV 2 acts as the reference vehicle (Yang et al., 2014), and the double-headed arrow means that there exists the bidirectional interaction between the related UAVs. Note that the defined altitude formation is zero for all $p_{Liz} = 0$, $i = 1, 2, 3, 4$. Thus, the local formation geometry of UAV 1 shown in Fig. 6, for instance, can be indicated as $\mathbf{p}_{L1} = (p_{L1x}, p_{L1y}, p_{L1z}) = (-150, -150, 0)$.

In order to maintain the overall formation stability during the multi-UAVs flight, it just needs to design decentralised formation controllers to stabilise all of the designed IASs, each of which is associated with an isolated UAV. As presented in Yang et al. (2012a), the feasible IASs were constructed and the longitudinal and lateral autopilots framework can be employed to design the longitudinal and lateral formation controllers for stabilising each IAS. Using the LMI-based H_∞ control methodology (Šiljak & Stipanović, 2000; Yang et al., 2014), the calculated state-feedback gain matrices of the longitudinal and lateral IASs are given by (36).

$$\begin{aligned} K_{long} &= \begin{bmatrix} 0.0455 & -0.1056 & 0.0890 & 4.7866 & 0.4322 & -0.0002 & -0.0055 & -0.1031 \\ -0.1487 & -0.0114 & 0.0094 & 0.2249 & -0.0716 & -0.0008 & 0.3373 & -0.0131 \end{bmatrix} \\ K_{lat} &= \begin{bmatrix} 0.0157 & 0.0119 & -0.0746 & 0.0970 & 0 & 0.0481 & -0.0146 \\ -0.0131 & -0.0081 & 0.0719 & -0.0166 & 0 & -0.063 & -0.0026 \end{bmatrix} \end{aligned} \tag{36}$$

Furthermore, the longitudinal and lateral compensators were designed heuristically to eliminate the corresponding steady-state formation error, and are listed in Table 2. Due to lack of space, please refer to Yang et al. (2012a) for the comprehensive treatment.

The simulated 3-D flight trajectories of the UAVs are shown in Fig. 7, and its planar projection is given in Fig. 8 to illustrate the longitudinal and lateral formation dynamics. Furthermore, the important indicator, LFEs associated with the mesh topology in Fig. 6 are displayed in Fig. 9 respectively.

As shown in these figures, the following observations can be made:

(1) The multi-vehicle formation in the forward, lateral and altitude directions remained stable during the turning manoeuvres and successfully tracked all the given waypoints in 3-D space.
(2) As shown in Fig. 9, during the turning manoeuvres, there existed the transient formation errors in the forward, lateral and altitude directions due to the desired cooperative turning flight. All these formation errors asymptotically converged to zero over time.

In conclusion, the flight formation of the multi-UAVs can be stabilised through stabilising all the associated IASs, and this verifies the formation stability result achieved in this paper.

6. Concluding remarks

Based on the formation error and the formation stability definitions, the formation stability hypothesis is proposed, and the EDA strategy is then specified to support the study of the formation control problem. Throughout the mathematical stability analysis and the simulation studies, it is concluded that the stabilisation of all the IASs is sufficient to guarantee the stability of the overall formation system.

However, there inevitably exists uncertain time-delay and formation error propagation in this method when neighbouring vehicles exchange information. These uncertainties do affect the stability of the system but is not modelled in the current scheme for simplicity. In this paper, since the presented formation stability analysis and the related stability theory are based on ideal communications between the vehicles, this method may not be directly applicable to physical systems. It is hoped that the discussion of formation stability with ideal communication channels here could provide a novel thought to conduct further stability analysis under the effect of time-delay, dynamic formation topology, formation error propagation, etc. The effect of these to the overall formation system will be investigated through mathematical analysis, simulations and experiments in our future work.

References

Askari, A., Mortazavi, M., & Talebi, H. (2013). UAV formation control via the virtual structure approach. *Journal of Aerospace Engineering*. (DIO:10.1061/(ASCE)AS.1943-5525.0000351)

Balch, T., & Arkin, R. (1998). Behavior-based formation control for multi-robot teams. *IEEE Transactions on Robotics and Automation*, *14*, 926–939.

Baldonado, M., Chang, C.-C. K., Gravano, L., & Paepcke, A. (2003). Aeronautical simulation block set V1.2, users guide [Computer software manual]. Unmanned Dynamics.

Corfmat, J., & Morse, A. (1976). Decentralized control of linear multivariate systems. *Automatica*, *12*, 476-495.

Desai, J. P., Ostrowski, J. P., & Kumar, V. (2001). Modeling and control of formations of nonholonomic mobile robots. *IEEE Transactions on Robotics and Automation*, *17*(6), 905–908.

Do, K. D. (2007). Bounded controllers for formation stabilization of mobile agents with limited sensing ranges. *IEEE Transactions on Automatic Control*, *52*(3), 569-576.

Dörfler, F., & Francis, B. (2010). Geometric analysis of the formation problem for autonomous robots. *IEEE Transactions on Automatic Control*, *55*(10), 2379-2384.

Fax, J. A., & Murray, R. M. (2004). Information flow and cooperative control of vehicle formations. *IEEE Transactions on Automatic Control*, *49*, 1465–1476.

Feddema, J. T., Lewis, C., & Schoenwald, D. A. (2002). Decentralized control of cooperative robotic vehicles: theory and application. *IEEE Transactions on Robotics and Automation*, *18*(5), 852–864.

Hong, Y., Gao, L., Cheng, D., & Hu, J. (2007). Lyapunov-based approach to multiagent systems with switching jointly connected interconnection. *IEEE Transactions on Automatic Control*, *52*(5), 943-948.

Khalil, H. K. (2001). *Nonlinear systems*. Prentice Hall, 3 edition.

Krick, L., Broucke, M. E., & Francis, B. A. (2009). Stabilisation of infinitesimally rigid formations of multi-robot networks. *International Journal of Control*, *82*(3), 423-439.

Li, N., & Liu, H. (2008, June 11-13). Formation UAV flight control using virtual structure and motion synchronization. In *Proc. American Control Conference, Seattle, Washington, USA* (pp. 1782–1787).

Lin, Z., Wang, L., Han, Z., & Fu, M. (2014). Distributed formation control of multi-agent systems using complex laplacian. *IEEE Transactions on Automatic Control*. (DIO:10.1109/TAC.2014.2309031)

Mesbahi, M., & Hadaegh, F. Y. (2000). Formation flying control of multiple spacecraft via graphs, matrix inequalities, and switching. *Journal of Guidance, Control, and Dynamics*, *24*(2), 369-377.

Monteiro, S., & Bicho, E. (2010). Attractor dynamics approach to formation control: theory and application. *Autonomous Robots*, *29*, 331–355.

Murray, R. M. (2007). Recent research in cooperative control of multi-vehicle systems. *Journal of Dynamic Systems, Measurement, and Control*, *129*(5), 571-583.

Ögren, P., Egerstedt, M., & Hu, X. M. (2002). A control Lyapunov function approach to multiagent coordination. *IEEE Transactions on Robotics and Automation*, *18*(5), 847–851.

Šiljak, D. D., & Stipanović, D. M. (2000). Robust stabilization of nonlinear systems: The LMI approach. *Mathematical Problems in Engineering*, *6*, 461–493.

Wang, J., & Wu, H. (2012). Leader-following formation control of multi-agent systems under fixed and switching topologies. *International Journal of Control*, *85*(6), 695–705.

Wang, J., & Xin, M. (2013). Integrated optimal formation control of multiple unmanned aerial vehicles. *IEEE Transactions on Control System Technology*, *21*(5), 1731–1744.

Wang, W., & Slotine, J.-J. E. (2006). A theoretical study of different leader roles in networks. *IEEE Transactions on Automatic Control*, *51*(7), 1156-1161.

Wu, Y., Cao, X., Xing, Y., Zheng, P., & Zhang, S. (2010). Relative motion coupled control for formation flying spacecraft via convex optimization. *Aerospace Science and Technology*, *14*(6), 415-428.

Xue, D., Yao, J., Chen, G., & Yu, Y. L. (2010). Formation control of networked multi-agent system. *IET Control Theory and Application*, *4*(10), 2168-2176.

Yang, A., Naeem, W., Irwin, G. W., & Li, K. (2012a, September 3-5). A decentralised control strategy for formation flight of unmanned aerial vehicles. In *Proc. 2012 UKACC International Conference on Control, Cardiff, UK* (pp. 345–350).

Yang, A., Naeem, W., Irwin, G. W., & Li, K. (2012b, June). Novel decentralised formation control for unmanned vehicles. In *Proc. IEEE Intelligent Vehicles Symposium (IV 2012), in Alcalá de Henares, Spain* (pp. 13–18).

Yang, A., Naeem, W., Irwin, G. W., & Li, K. (2014). Stability analysis and implementation of a decentralised formation control strategy for unmanned vehicles. *IEEE Transactions on Control Systems Technology*, *22*(2), 706–720.

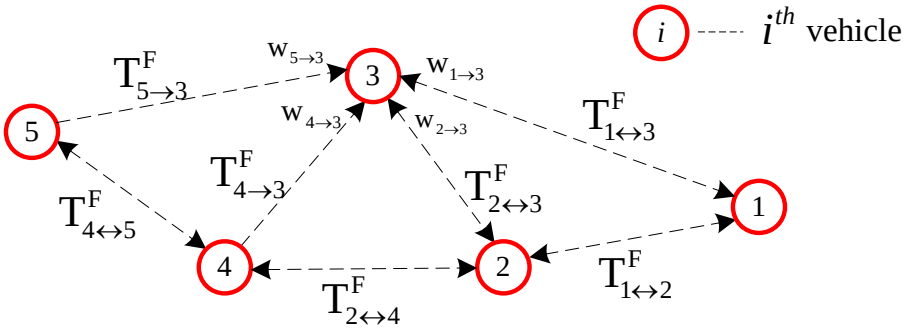

Figure 1. Mesh formation topology with unidirectional and bidirectional reactions

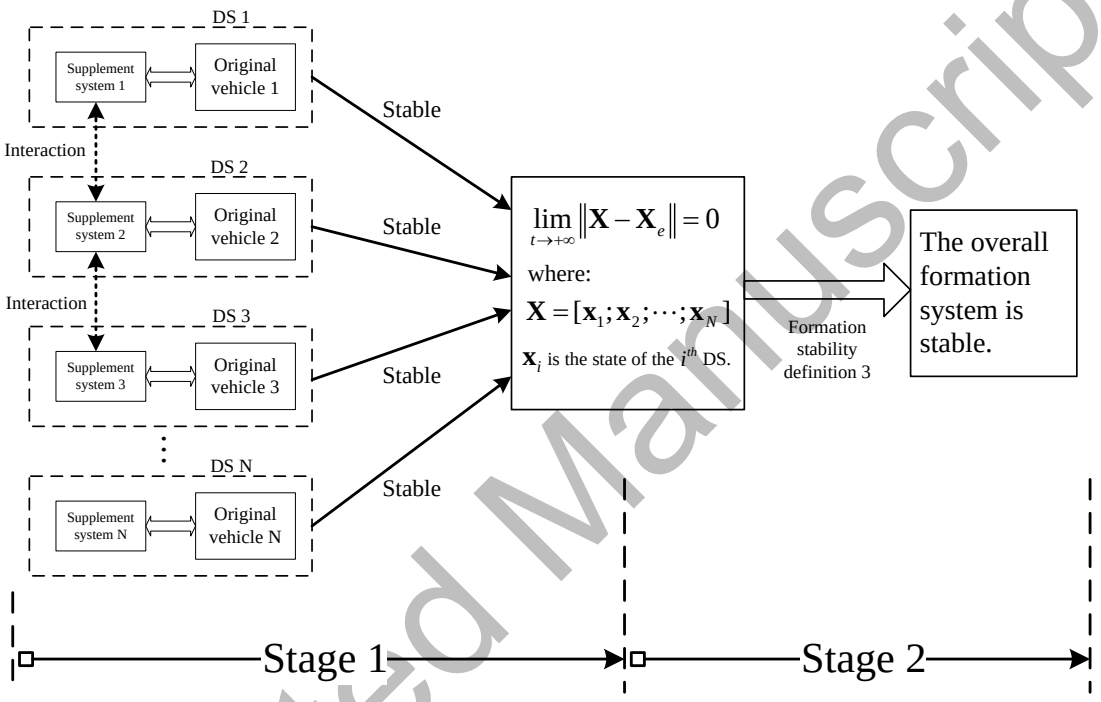

Figure 2. Analysis process of the formation stability based on the hypothesis

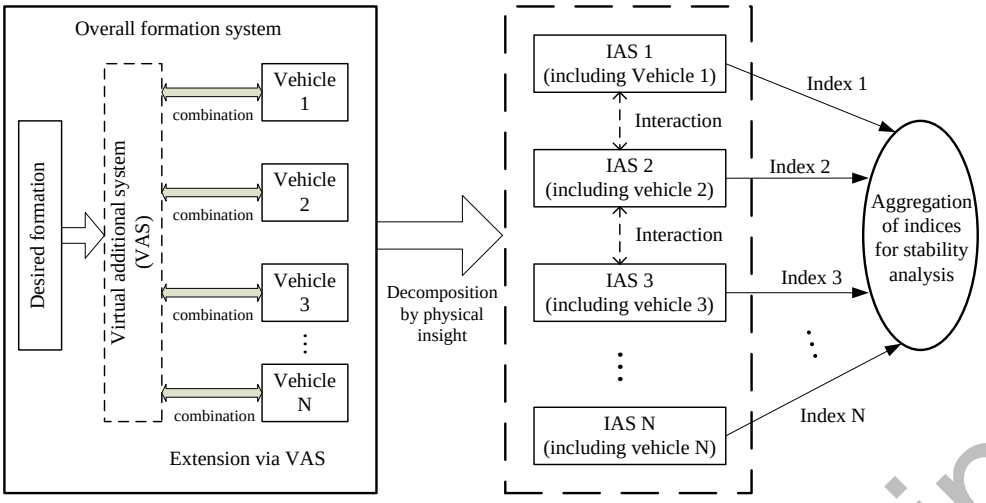

Figure 3. Process of extension-decomposition-aggregation

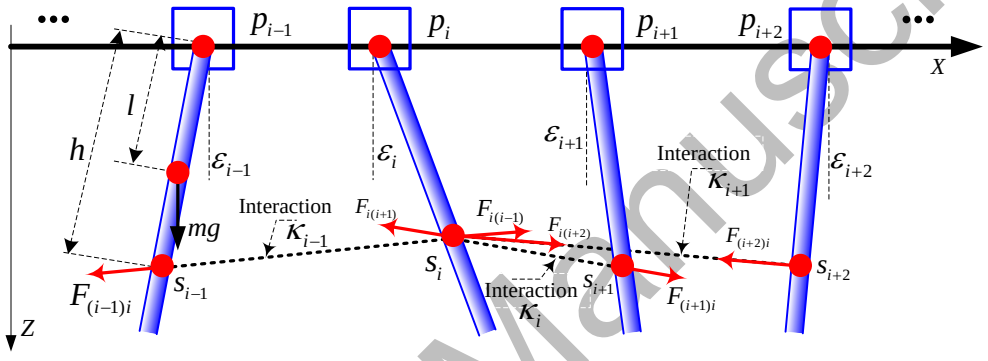

Figure 4. Coupled-multiple-pendulum system

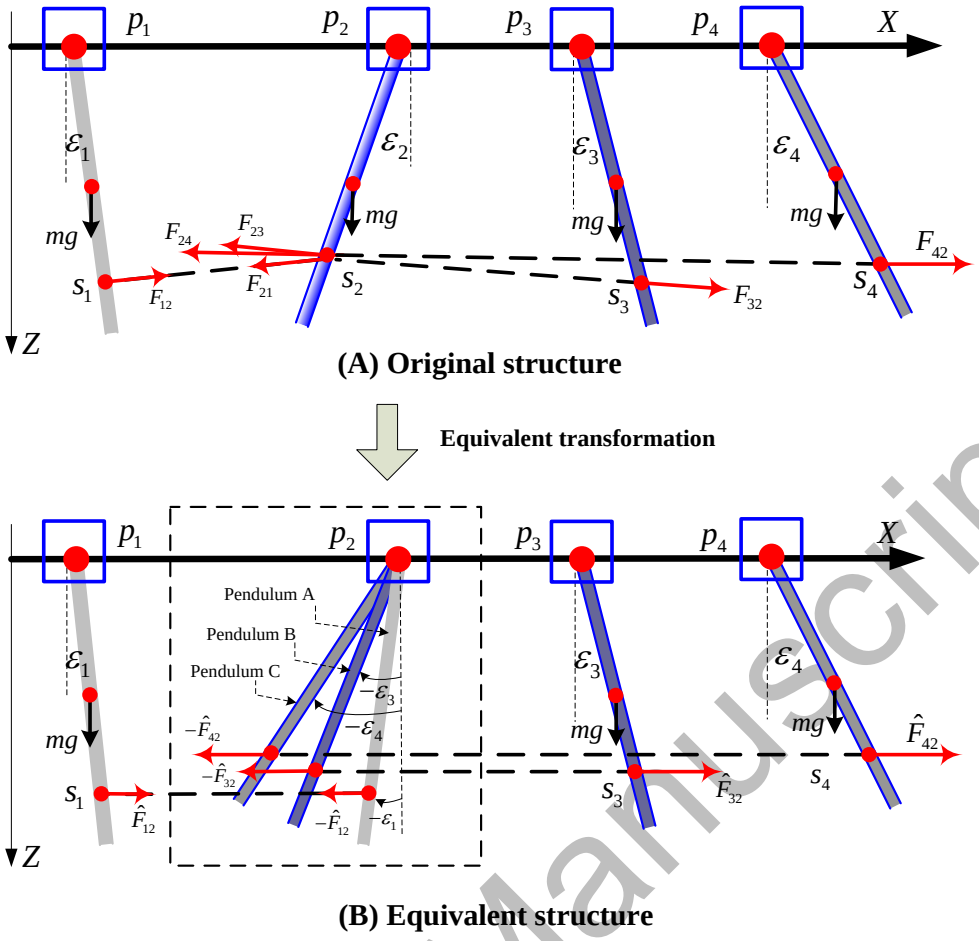

Figure 5. Equivalent transform diagram

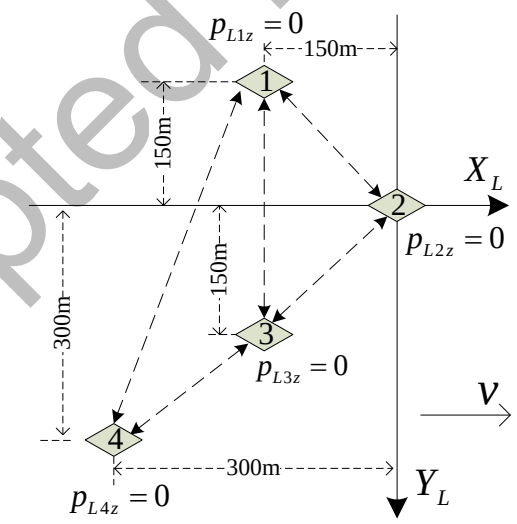

Figure 6. Formation geometry and mesh topology of UAVs in LFCS

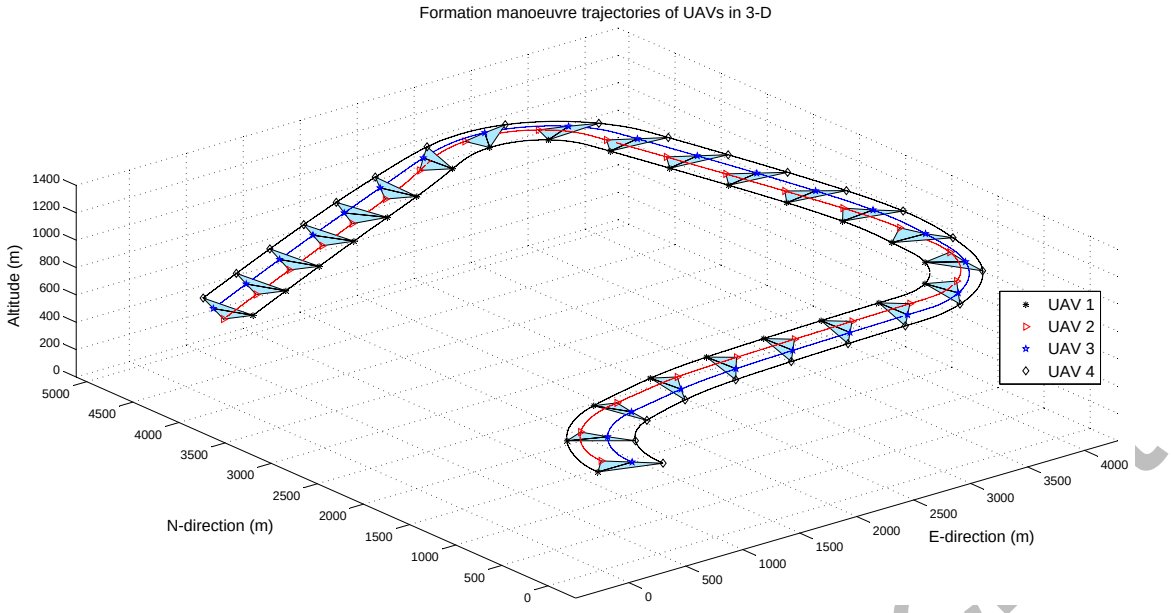

Figure 7. Motional trajectories of the UAVs formation in 3-D space

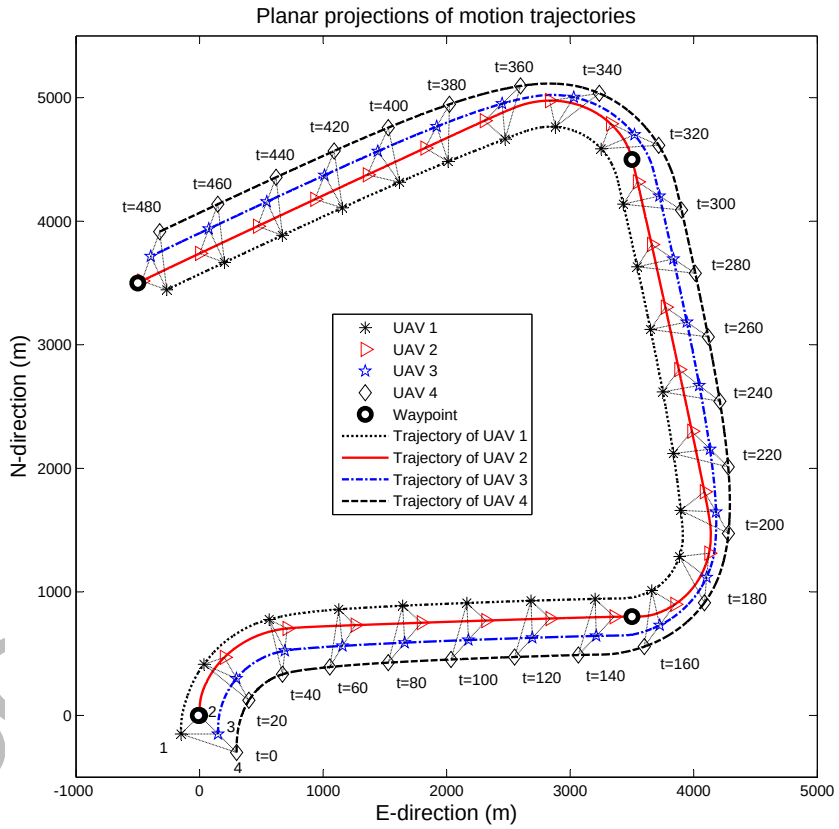

Figure 8. Planar projections of 3-D trajectories of UAVs formation corresponding to Fig. 6

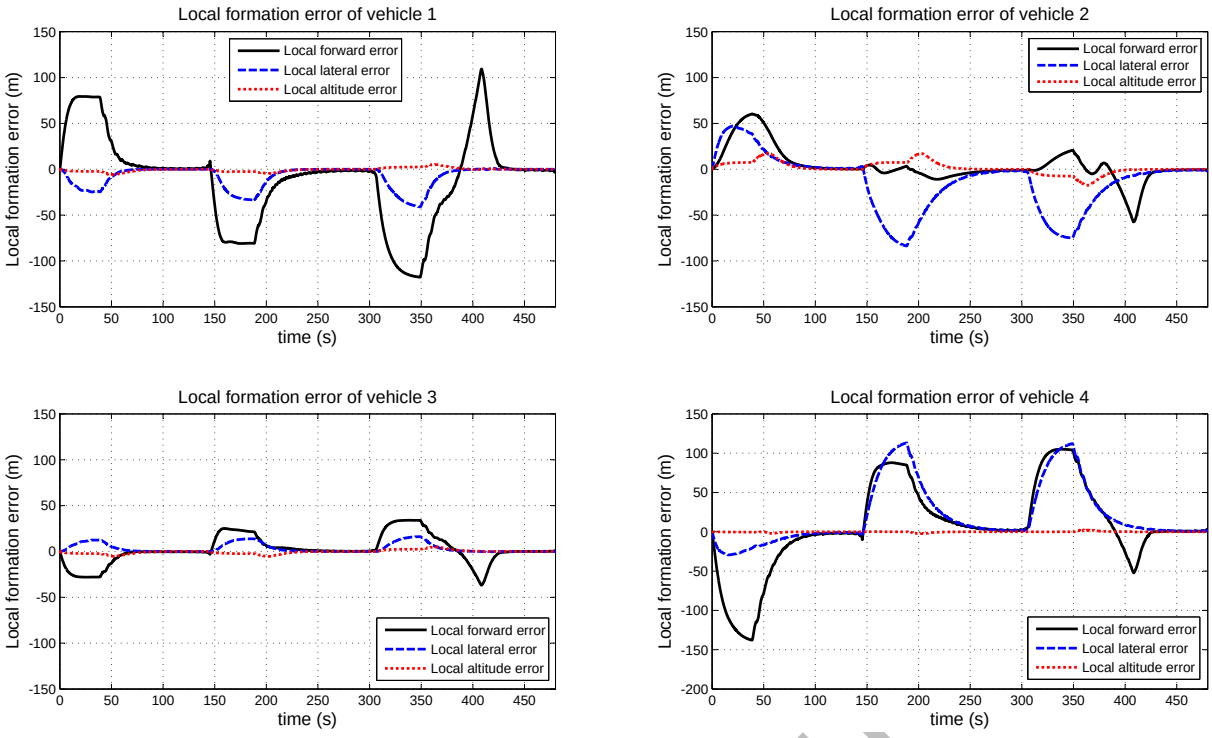

Figure 9. Formation error dynamics of UAVs during turning manoeuvre

Table 1. Predefined 3-D waypoints of UAVs formation manoeuvre

Number	1	2	3	4
$North(m)$	0	800	4500	3500
$East(m)$	0	3500	3500	-500
$Altitude(m)$	800	900	1000	900

Table 2. PI parameters of all the compensators

Lateral compensators			Longitudinal compensators		
Variables	K_p	K_i	Variables	K_p	K_i
ϕ	1.0	2.0	H	0.13	0.7
ψ	0.5	2.0	V	0.4	0.25
ε_{lat}	0.15	3.80	ε_{long}	0.5	4.0